THE PENNSYLVANIA STATE UNIVERSITY
SCHREYER HONORS COLLEGE

DEPARTMENT OF BIOCHEMISTRY AND MOLECULAR BIOLOGY

Assessing the Adaptability of Neonatal Herpes Simplex Virus Type 2 to Different Host Cell Types

ELLIE KIM
SPRING 2023

A thesis
submitted in partial fulfillment
of the requirements
for baccalaureate degrees
in Biochemistry and Molecular Biology and Music
with honors in Biochemistry and Molecular Biology

Reviewed and approved* by the following:

Moriah Szpara
Associate Professor of Biology
Thesis Supervisor

Lorraine Santy
Associate Professor of Biochemistry and Molecular Biology
Honors Adviser

* Electronic approvals are on file.

ABSTRACT

Herpes simplex virus type 2 is a common sexually transmitted infection that rarely causes death in adults, but it can produce severe disease for neonates. The severity of HSV-2 infection in neonates is very diverse, ranging from mild skin infections to fatal brain inflammation. Currently, it is not understood why infections with some strains of HSV-2 are more virulent, while other strains produce attenuated phenotypes in their hosts. In this project, two strains that produced a disseminated infection phenotype (C1-11 and C2-80) were analyzed in their ability to adapt to different host cells in a laboratory setting. We showed that viral adaptation happens quickly within two to three passages in cell culture, leading to enhanced plaque formation and cell-cell spread for both strains. Whole genome sequencing revealed few genetic changes occur as these viruses adapt over just a few days in culture. These results demonstrate the necessity for well-controlled environments when comparing various strains of HSV-2, as differences in growth conditions and environment have drastic effects on their phenotype. In addition, there were notable differences between strains in their ability to adapt to their respective environment. Strain C2-80 had larger plaques, areas of spread, viral load, and viral titers. These observations suggest that differences in adaptability *in vitro* may be an important factor that distinguishes between virulent and attenuated strains. The results from this study contribute to establishing phenotypic and genotypic profiles of neonatal HSV-2 infections to help build associations between these data and the severity of a given strain. The ability to predict the severity of an infection by characterizing the viral strain could be one approach to reducing HSV-2 neonatal infant mortality and debilitating disease.

TABLE OF CONTENTS

LIST OF FIGURES

LIST OF TABLES

ACKNOWLEDGEMENTS

I would like to thank Dr. Moriah Szpara for the opportunity to engage with the research in her lab. The experience she provided me was one of my first endeavors into wet-bench research, springing me into a journey of molecular biology research throughout my college career at Penn State. I would like to thank my graduate student mentor, Sarah Dweikat, for her continued support in designing this senior thesis project. Her patience in answering many of my questions was what allowed me to grow as a scientist over the years. Thank you to Chris Bowen for preparing the virus samples used throughout this thesis, and thank you to Daniel Renner and Sarah Dweikat who played a large role in assembling the genomes of these viruses. Thank you to the rest of the Szpara lab for their guidance in understanding new protocols, helping me find reagents, and their support in my endeavors. I would also like to thank our collaborator, Dr. Lisa Akhtar, who is currently at the Northwestern University Feinberg School of Medicine, for sharing samples of neonatal herpes simplex virus for this project.

Chapter 1

Introduction

Herpes simplex virus type 2 (HSV2) is a common sexually transmitted infection affecting 22% of the population in the US. Typical symptoms include sores, blisters, ulcers, and urinary tract infections, as it is mostly found in the genital niche[1]. On the other hand, HSV1 is commonly found in the oral niche with symptoms such as oral lesions, but it can also cause genital infection similar to HSV-2. Infection by both HSV 1 and 2 is usually mild but can persist for a lifetime as the virus establishes latency in neurons and can later reactivate from these cells. When a mother is shedding virus in the genital tract, non-sexual transmission can occur from mother to child during birth. In neonates (babies of 1 month or younger), infections can present with symptoms ranging from mild sores and ulcers on the skin, to fatal inflammation of the brain and spinal cord, or invasion of other organ systems such as the liver and lungs[2]. HSV-2 is predominantly the cause for neonatal infections: out of 14,000 neonatal HSV infections anaually, 10,000 are a result of HSV-2 infections[3]. About half of these HSV-2 cases are relatively mild infections localized to the skin, eye, and mouth (SEM), but the other half are more invasive[4]. About 30% of neonatal HSV cases are disseminated infections, with mortality rates of 85% by age 1[4]. Lastly, about 15% of cases show signs of inflammation to the brain and spinal cord, known as central nervous system (CNS) infections. Disseminated and CNS infections are the most severe form of infection that may be fatal in young babies. Though most disseminated and CNS cases are treatable with acyclovir, many surviving neonates have long-lasting neurological damage and life-long symptoms[4]. Current medical protocols recommend various dosages of acyclovir, based

on shedding frequency and symptom recurrence rates[5]. If the severity of the infection can be predicted at the time of birth or infection, physicians may be able to create new guidelines to tailor prescription dosages to the predicted disease severity, rather than waiting to assess post-infection outcome. Characterizing HSV-2 strains into high or low virulence categories, especially in neonates, is one of the first steps to overcoming this diagnostic challenge.

Significance of Genomic Analysis in HSV Research

With recent analyses of HSV genomes across the globe, HSV was revealed to have vast diversity in its genome across the globe. This diversity has arisen despite their stable DNA genomes[6]. The differences that occur between individual viral strains could be one reason for the differences in symptom severity and type. For example, figure 1 shows the genetic diversity that is present in HSV-1 and HSV-2, to exemplify the noticeable genetic differences between strains and species. Though HSV-1 has the greatest diversity in strain-to-strain genome, HSV-2 also exemplifies a similar pattern in the star-shaped nature of the gene network tree, unlike VZV which is another related virus in the *Herpesviridae* family.

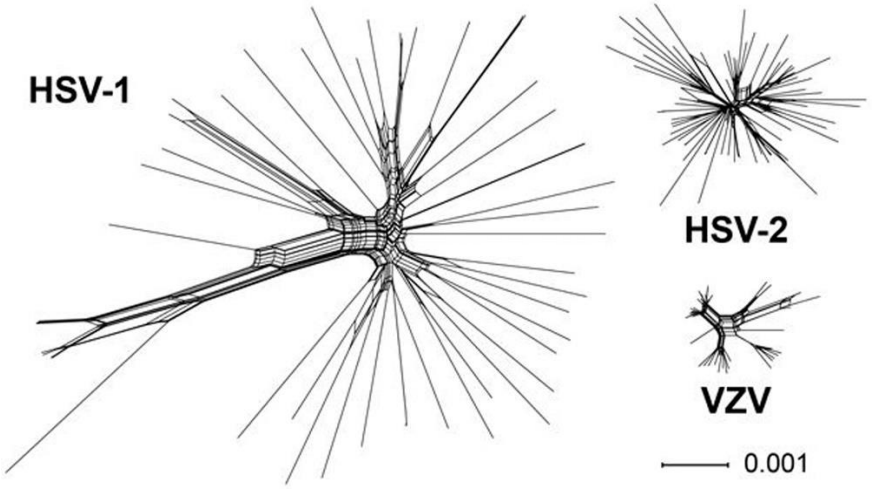

Figure 1: Genetic diversity in HSV-1 and HSV-2.

The whole genome sequence of various HSV-1, HSV-2, and VZV strains were aligned by SplitsTree to highlight the genetic diversity in each virus. Each line represents one strain of HSV-1, HSV-2, or VZV. The scalebar represents the number of nucleotide differences per position. HSV-1 has the largest diversity indicated by the larger graph, with HSV-2 also having a relatively diverse genome indicated by the widely spread web shape. VZV, a closely related virus in the *Herpesviridae* family, has relatively little diversity in genome as strains cluster closer together in this network. This figure was reproduced from published work, Kuny, et al., 2020[7]. doi: 10.21775/cimb.042.041

There have been specific genes like gB and gI which have been highlighted as being crucial to permitting faster spread of the virus, but it is unclear what variants lead a few select strains to develop into more severe infections[8]. Though many strains of HSV-1 and 2 have been sequenced, there is currently no defined guideline to precisely predict the severity of a particular strain based solely on its genome.

Viral Growth in Cell Culture

One method of characterizing HSV strains in the laboratory is to grow HSV in mammalian cell culture to understand its cytopathic effect. When HSV 1 or 2 is introduced to a monolayer of mammalian cells in culture, the virus creates plaques, or visible areas of cell death over its course of infection. Small plaques can indicate inefficient viral release, replication, entry, or cell-cell spread, while large plaques may indicate higher efficiency of these processes[9]. Studies of HSV-1 in cell culture have revealed adaptations that occur among viruses in cell culture, which are dependent on genetic differences that manifest as phenotypic shifts. Over ten passages in cell culture, a mixed population of HSV-1 selects for larger plaques and syncytia[10]. Passaging is the process of creating a viral stock in a population of cells. This phenomenon of lab adaptation may also be true for HSV-2 clinical isolates. In a particular clinical isolate, the population of HSV is not uniform; rather there are minor variants that may make a particular virion unique. Because of this viral diversity, environmental pressures, including the ones in laboratory cultures, may result in a shift in phenotype over time. Studying how these viruses behave in cell culture may be one method to understanding viral behavior and pathogenicity.

This project aims to understand the behavior of low-passage neonatal HSV-2 strains in laboratory cell culture to assess their adaptability to new host cell environments. Two neonatal HSV-2 strains were chosen as the focus of this project: C1-11 and C2-80. Strain C1-11 came from a female neonate who had disseminated HSV-2 infection at 8 days old. The sample was collected from the serum at 11 days old. Strain C2-80 came from a female neonate who also had disseminated HSV-2 infection at 12 days old. The sample was collected on the day of diagnosis from the plasma. These clinical isolates were cultured on African green monkey kidney (Vero) cells and human lung fibroblast (MRC5) cells (figure 2) in parallel. Vero cells are commonly

used in virology laboratories to obtain a baseline understanding of the viral phenotype in the absence of an immune response element, as these cells lack interferon responses to infection[11]. MRC5 cells are a human cell line that may be a more accurate representation of how viruses may behave in a human system. The samples were grown on two different cell types to assess how their initial environment affects viral behavior.

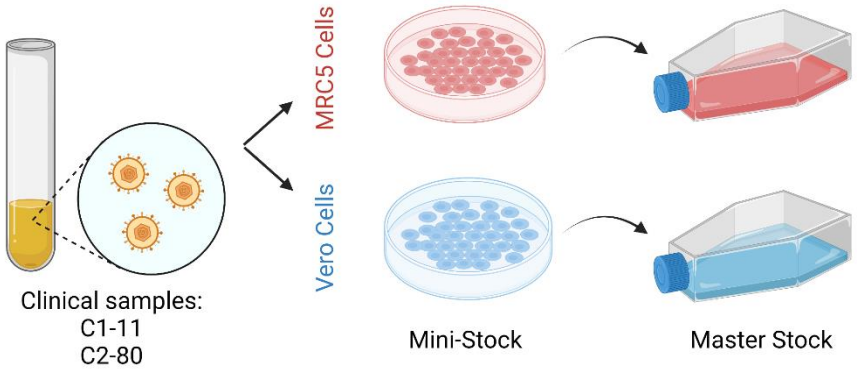

Figure 2: *In vitro* growth of clinical HSV samples.

The serum or plasma containing HSV-2 from the patient was grown in a mini-stock to calculate viral titer, and then grown in a larger master stock for propagation. This process was performed on both Vero and MRC5 cells. Image created using BioRender.

Previous studies of neonatal HSV-2 infections revealed that strains coming from CNS infections tended to create larger areas of cell-cell spread[12]. These areas are detected by indirect immunofluorescence as they are the regions that HSV-2 spread to beyond the plaque boundaries that were visible by methylene blue staining. Throughout this paper, the plaque borders visible by methylene blue staining will be referred to as "plaque area" and the borders visible by immunofluorescence staining will be referred to as "spread area." Spreading faster and more extensively in a host may be indicative of higher fitness and virulence. As seen in figure 3, two out of three CNS infections shown have larger areas of spread at 72 hours post-infection than the

SEM infection. The ability to characterize differences between viral strains is crucial to building a strong foundation to predict the severity of infection of a given strain. The HSV-2 strains of interest in this study, C1-11 and C2-80, were analyzed by plaque assay, indirect immunofluorescence, and genome analysis to understand strain-to-strain differences. C1-11 and C2-80 strains come from infections of similar severity as disseminated infections, so I hypothesized that these strains would have similar laboratory profiles with similar plaque size, cell-cell spread, and the ability to adapt quickly to a changing environment.

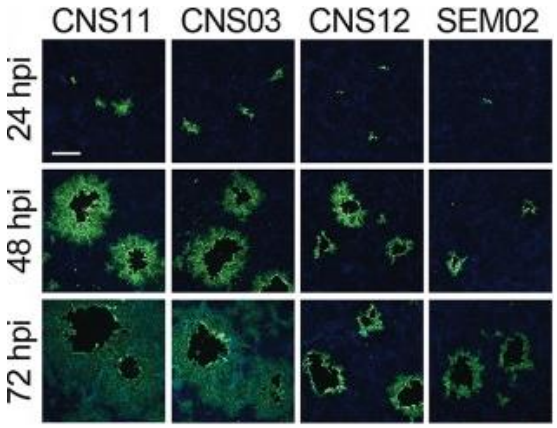

Figure 3: Cell-cell spread of neonatal HSV-1 differs based on clinical severity.

The green fluorescence shows the presence of HSV by indirect immunofluorescence. At 72 hours, there are noticeable differences in cell-cell spread as most of the CNS strains exhibit a large ring of spread around the focus of infection. This figure was reproduced from published work, Akhtar, et. al., 2019[12]. doi: 10.1128/mSphere.00590-18

Chapter 2

Results

Image Analysis of MRC5-Grown Strains

Initial analyses of the C1-11 and C2-80 strains were done using the MRC5-grown samples to understand plaque phenotype and cell-cell spread. These samples had been grown on MRC5 cells to obtain a mini-stock, master-stock, and a working-stock. They were then grown on Vero cells to observe their plaque phenotype. Throughout the rest of the thesis, these samples will be named MRC5-Vero, where the first cell type (MRC5) is the cell type that the strains were passaged on and the second is the cell type (Vero) that the virus strain was observed in. Figure 4 shows that both virus strains create small plaques, where cell death can be observed by the dark aggregate of cells shown in both panels. C1-11 MRC5-Vero plaques had a mean area of 0.027 mm^2 (n=33) and C2-80 MRC5-Vero plaques had a mean area of 0.050 mm^2 (n=113). C2-80 has a slightly larger plaque area ($p = 0.0045$ by two-sampled t-test assuming unequal variance), but the overall phenotype of these two strains are similar, creating dense and irregular plaques on Vero cells.

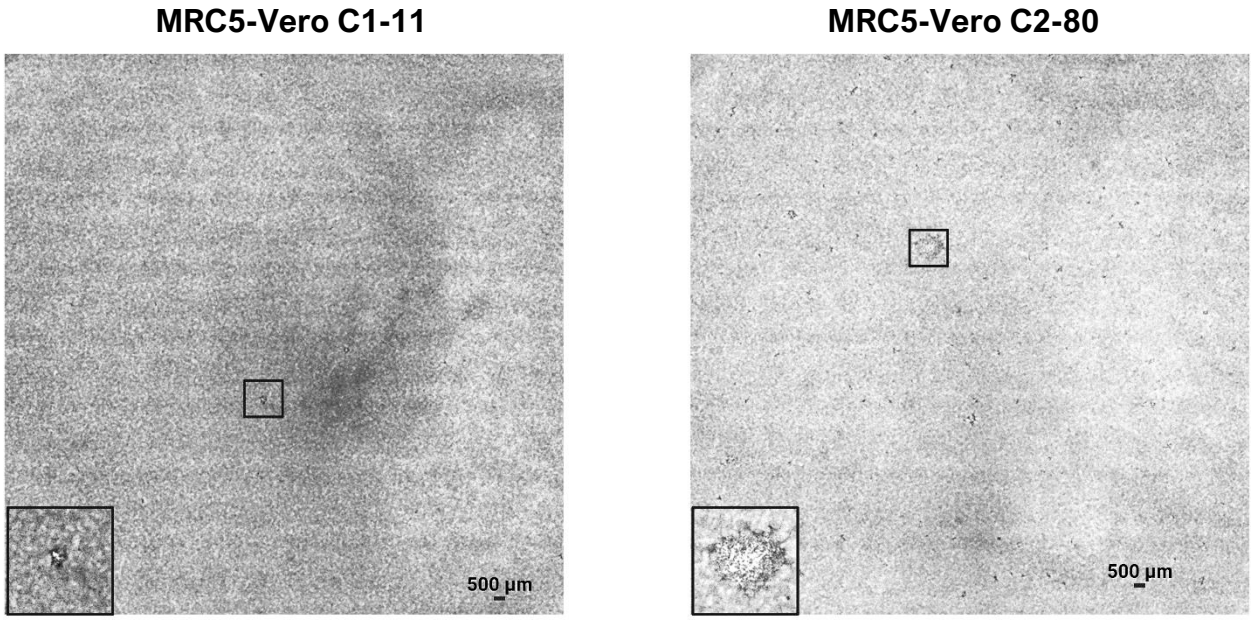

Figure 4: Plaque assay of MRC5-grown C1-11 (left) and C2-80 (right) shows similar small-plaque phenotypes.

Vero cells were infected with HSV-2 strains and incubated for 72 hours under DMEM and methylcellulose prior to staining with methylene blue in methanol. Both MRC5-grown strains of C1-11 and C2-80 show very small plaques, as seen by the dark aggregates of cells (shown in the zoomed slides). The mean area of C1-11 plaques were 0.027 mm^2 while C2-80 plaques were 0.050 mm^2. Though they are both small, there was a significant different between the two groups ($p = 0.0045$ by two-sampled t-test assuming unequal variance). The scalebar indicates 500 µm and the images are of the whole 35 mm plate, with 8x8 tiling at a 4x zoom. The darker area on the left image may be due to greater cell density in that region, not due to higher viral content.

In addition to plaque assay, indirect immunofluorescent imaging was used to evaluate the extent of cell-cell spread exhibited by the C1-11 and C2-80 MRC5-Vero samples. An anti-HSV antibody (Dako) was used as the primary antibody to locate the HSV particles while a Cy5 fluorescent secondary antibody was used to detect the primary antibody, as shown in red in figure 5. The average area of C1-11 MRC5-Vero plaques was 0.065 mm^2 (n=189) and C2-80 MRC5-Vero was 0.074 mm^2 (n=92). Consistent with the plaque assay, these two strains have similar areas of spread and exhibit a similar small and irregular phenotype.

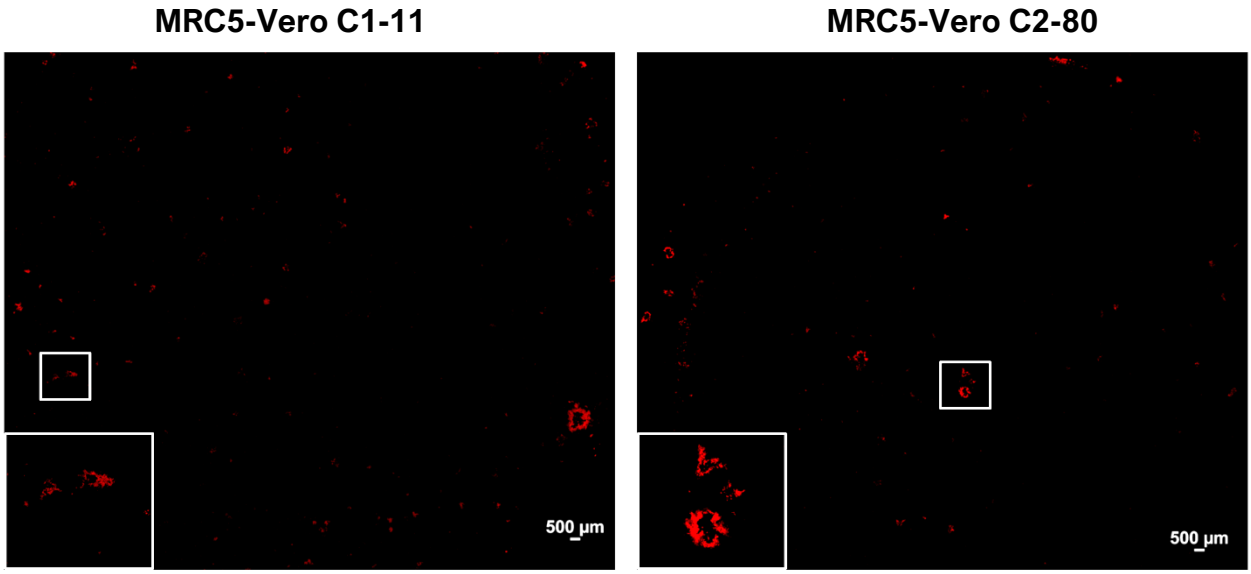

Figure 5: Indirect immunofluorescent staining shows tight borders around the focus of infection for MRC5-grown C1-11 (left) and C2-80 (right).

Vero cells were infected with HSV-2 strains and incubated for 72 hours under human serum and DMEM prior to indirect immunofluorescent staining. Anti-HSV antibody and a Cy5 fluor (shown in red) was used to image locations of HSV to observe the ring of infection around a focus. Both MRC5-grown strains of C1-11 and C2-80 show tight borders of infection around a focus, but C2-80 tended to have larger areas of total spread, or the area within the outermost border of infection. The mean area of C1-11 spread was 0.065 mm^2 and C2-80 was 0.074 mm^2. The scalebar indicates 500 µm and the images are of the whole 35 mm plate, with 8x8 tiling at a 4x zoom.

Image Analysis of Vero-Grown Strains

Though the plaque phenotypes of both C1-11 and C2-80 were small when these strains were introduced newly into Vero cells, both strains' phenotypes changed dramatically when the Vero-grown strains were observed. In these Vero-Vero samples, the strains were passaged through Vero cells for the mini, master, and working stocks and then allowed to form plaques on Vero cells. In total, they had three passages in Vero cells prior to the plaque-visualization step.

In the plaque assay (figure 6), the Vero-Vero plaques appear larger in size but more circular in shape for both viral strains. C1-11 Vero-Vero has a mean area of 0.13 mm^2 (n=161) and C2-80 Vero-Vero has a mean area of 0.38 mm^2 (n=134). The C2-80 strain was significantly larger than the C1-11 strain ($p < 10^{-30}$).

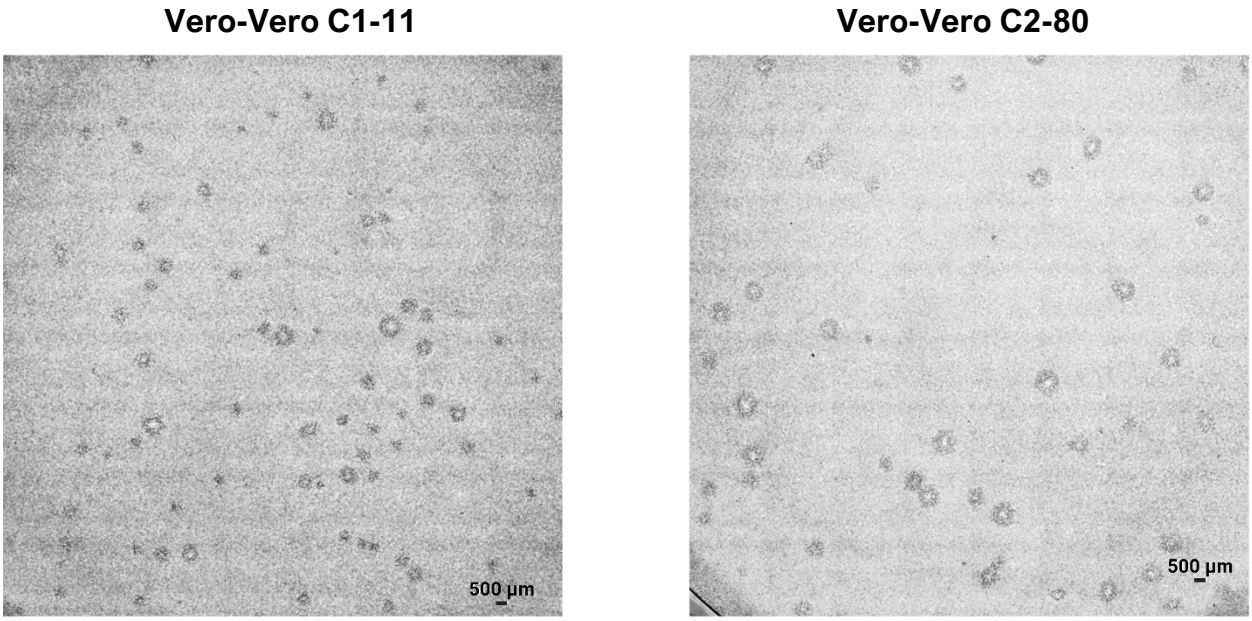

Figure 6: Plaque assay of Vero-grown C1-11 (left) and C2-80 (right) shows dramatically larger plaques after subsequent passaging in Vero cells.

Vero cells were infected with HSV-2 strains for 72 hours prior to staining with methylene blue in methanol. Both Vero-grown strains of C1-11 and C2-80 strains show larger and circular plaques, especially in comparison to their MRC5-grown counterparts in figure 4. At this point, these strains have been passaged in Vero cells for three times before the plaque assay in Vero cells. However, the strain C2-80 still retains its larger plaque size with a mean area of 0.38 mm^2 while C1-11 has a mean plaque size of 0.13 mm^2 ($p < 10^{-30}$ by t-test). The scalebar indicates 500 µm and the images are of the whole 35 mm plate, with 8x8 tiling at a 4x zoom.

Just as the plaque areas increased in the Vero-Vero examples, the spread areas have increased nearly proportionally. C1-11 Vero-Vero has an average area of 0.49 mm^2 (n=64) and C2-80 Vero-Vero is 0.58 mm^2 (n=49). C2-80 is consistently slightly larger than C1-11 in terms of plaque size and spread area in both MRC5-Vero and Vero-Vero samples. In the right panel of figure 7, there are many more smaller plaques around the larger plaques, which may indicate that these are "satellite plaques" formed from the virions produced from the larger "parent plaques." Many more satellite plaques are visible in the immunofluorescent imaging due to differences in how the infections were carried out (refer to Methods chapter). This presents a challenge in accurately quantifying the spread areas of the original plaques formed from the infection.

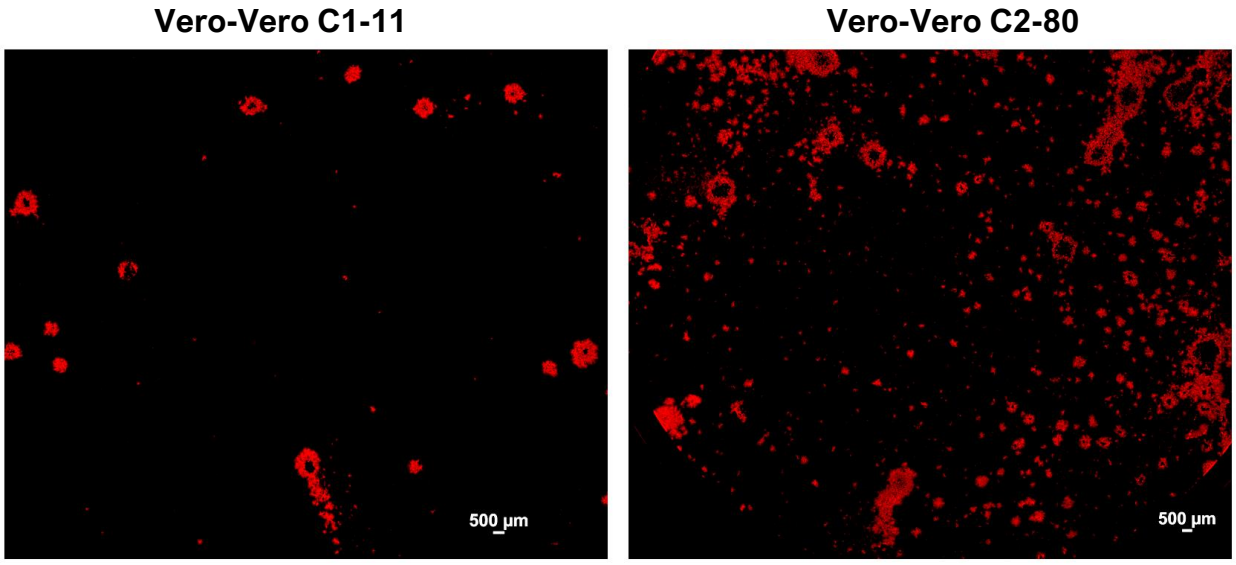

Figure 7: Indirect immunofluorescent staining of Vero-grown C1-11 (left) and C2-80 (right) shows greater cell-cell spread after subsequent passaging on Vero cells.

Vero cells were infected with HSV-2 strains and incubated for 72 hours under human serum and DMEM prior to indirect immunofluorescent staining. Anti-HSV antibody and a Cy5 fluor (shown in red) was used to image the extent of cell-cell spread exhibited by various strains of HSV-2. Both Vero-grown strains of C1-11 and C2-80 show greater spread in comparison to their MRC-5 grown counterparts in figure 5. C1-11 appears to have greater spread relative to its focus of infection, shown by the black center. C2-80 had a larger total spread area at a mean of 0.58 mm^2 while C1-11 averaged 0.49 mm^2. In both instances, smaller satellite plaques were present around a larger focus of infection, which may be secondary plaques formed as a result of viral particles spreading to nearby cells during incubation. The strains were not infected at the same MOI, which may attribute to the different numbers of plaques for the two strains. The scalebar indicates 500 µm and the images are of the whole 35 mm plate, with 8x8 tiling at 4x zoom.

Comparison of Vero-Grown to MRC5-Grown Strains

The tendency to show an increase in plaque size and spread area in Vero cells is clear in both C1-11 and C2-80 strains, as shown in figure 8. The Vero-Vero samples have a larger plaque area compared to the MRC5-Vero samples. For strain C2-80, the amount of spread increased consistently with its plaque area, highlighted in green in table 1. Strain C1-11 tended to increase its ratio of spread area to plaque area when it was kept in a consistent environment of Vero cells.

Table 1: C1-11 has larger cell-cell spread areas, relative to its plaque size.

	Mean Spread Area by immunofluorescence	Mean Plaque Area by methylene blue staining	Spread Area:Plaque Area
C1-11 MRC5-Vero	0.065 mm^2 (n=189)	0.027 mm^2 (n=33)	2.4
C1-11 Vero-Vero	0.49 mm^2 (n=64)	0.13 mm^2 (n=161)	3.7
C2-80 MRC5-Vero	0.074 mm^2 (n=92)	0.050 mm^2 (n=113)	1.5
C2-80 Vero-Vero	0.58 mm^2 (n=49)	0.38 mm^2 (n=134)	1.5

Though strain C2-80 was consistently larger in plaque size and cell-cell spread areas, strain C1-11 appears to have a greater capability to spread, relative to its plaque size. Strain C2-80 has a consistent spread area to plaque area ratio around 1.5, meaning that the cell-cell spread is proportional to its plaque size. However, C1-11 has a larger ratio; there is greater cell-cell spread for a given plaque size. Furthermore, this ratio increases for the sample that had been passaged in Vero cells multiple times, suggesting that its spread area increases as a result of adaptation to a particular host.

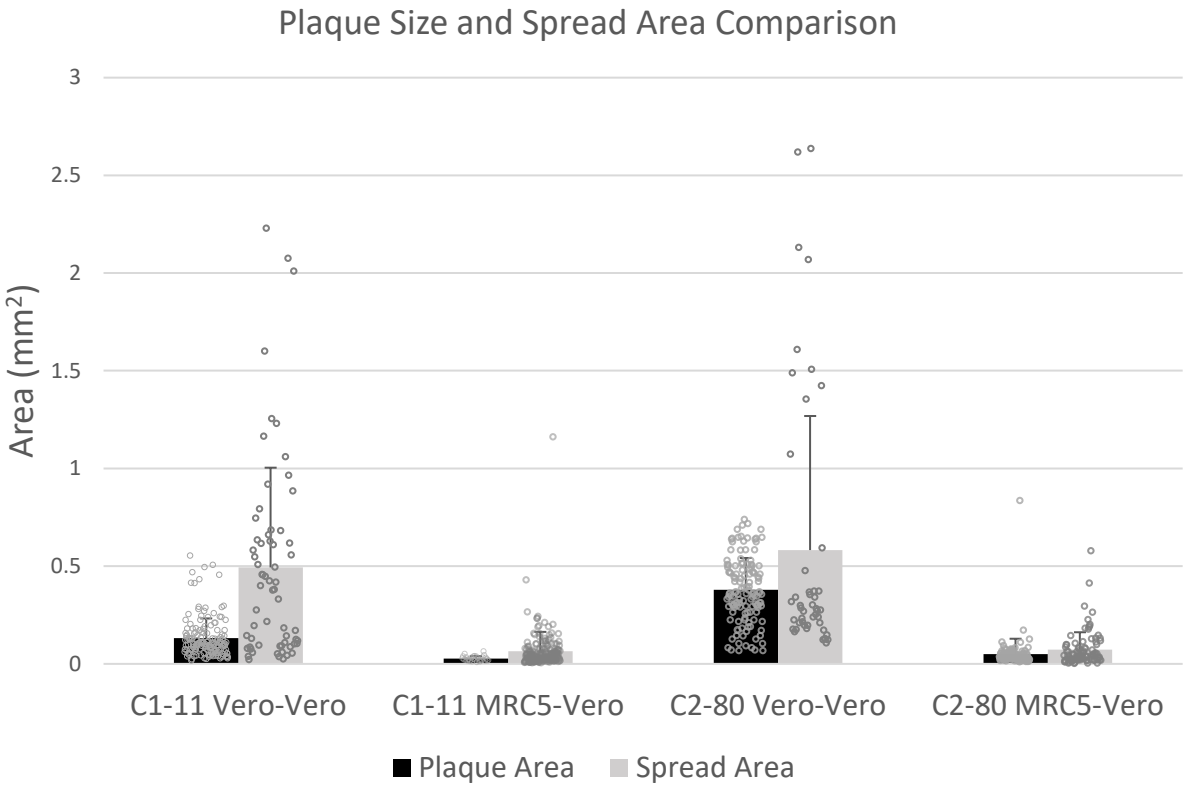

Figure 8: Introducing HSV-2 strains to a new host significantly decreases plaque size and cell-cell spread.

A comparison of Vero-grown strains against MRC5-grown strains showed significant differences between the two groups with respect to size and variation. Vero-Vero indicates that the strains were passaged in Vero cells for the mini, master, and working stocks and were also observed in Vero cells. MRC5-Vero indicates that the strains were passaged in MRC5 cells for the mini, master, and working stocks but were observed in Vero cells, a new host cell type. Each data point was plotted with bars to represent the mean of each sample. The error bars represent one standard deviation. A two sampled t-test assuming unequal variance revealed significant differences between the MRC5-Vero and Vero-Vero samples for both strains ($p < 10^{-5}$ for all MRC5-Vero to Vero-Vero comparisons). Refer to table 1 for numbers of plaques quantified for each strain.

Quantification of viral load by Western blot

Image analysis revealed that plaque sizes and spread areas increased over a few consistent passages in Vero cells. To understand if the amount of viral proteins produced is consistent with the observation of larger plaques, Western blots of the same strains were performed (figure 9). Vero-grown and MRC5-grown C1-11 and C2-80 strains were grown on Vero cells for a 24-hour infection period at a multiplicity of infection (MOI) = 0.01. In other words, the infection had one plaque forming unit (PFU) for every 100 Vero cells. The samples were collected in duplicate to ensure replicability. The Dako antibody detects multiple HSV surface proteins, and GAPDH was used as the loading control. Contrary to the larger plaque sizes and spread areas seen in the Vero-Vero samples, the MRC5-Vero infections appeared to have more HSV protein at this time point. However, this may not be true as it is suspected that the viral titer for the MRC5-Vero samples were inaccurate due to the possibility of undercounting the number of PFUs. This was confirmed later (table 2) when the titers in Vero and rabbit skin cells were compared. Based on the inconsistent loading and non-ideal polymerization of the gel, the Western blot did not yield conclusive results about the viral load of C1-11 or C2-80.

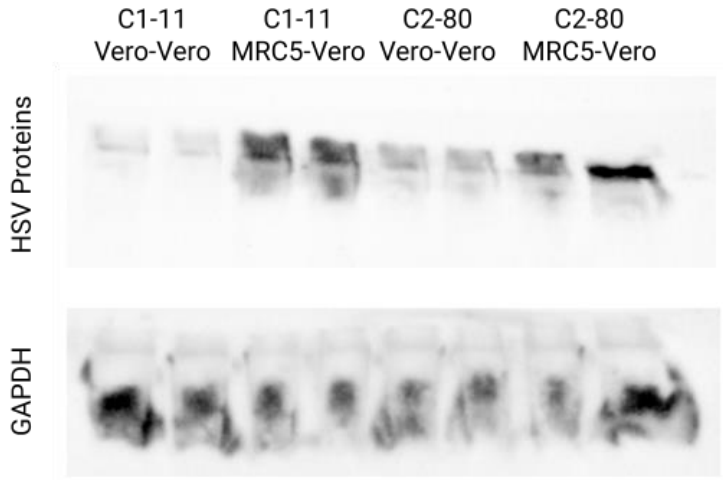

Figure 9: Western blot of HSV proteins shows inconsistent results of viral load for C1-11 and C2-80.

Vero cells were infected at a MOI of 0.01 for all samples (MRC5-grown and Vero grown C1-11 and C2-80 strains) and incubated for 24 hours under DMEM. The lysates were collected in RIPA buffer with DTT and protease inhibitor. The protein content was normalized by BCA assay prior to loading on the gel. The top image shows the anti-HSV stain, showing total viral load in each lane. The bottom image shows the anti-GAPDH stain as the loading control. The Vero-Vero samples seem to have less viral load, but this may be due to an error in calculating titers, addressed in table 2. Comparison between the viral load of C1-11 and C2-80 cannot be assessed due to inconsistent loading shown by the GAPDH stain.

Titer of C1-11 and C2-80 Strains on Vero and Rabbit Skin Cells

To confirm that the results of the Western blot was a true reflection of the viral quantity, and not an artifact of an inaccurate titer, the titers were compared between Vero and Rabbit skin cells. This is simply a repetition of the titering in Vero cells, just in a different cell type. In Vero cells, the MRC5-grown samples show very small plaques, which can easily be missed during plaque analysis. However, in rabbit skin cells, the plaques look large and uniform across strains and samples as seen in figure 10. This characteristic makes it easier to quantify how many PFU

there are in a given volume. Confirming that the titer in rabbit skin cells are equal to the titer in Vero cells allowed confirmation of the authenticity of the results of the Western blot.

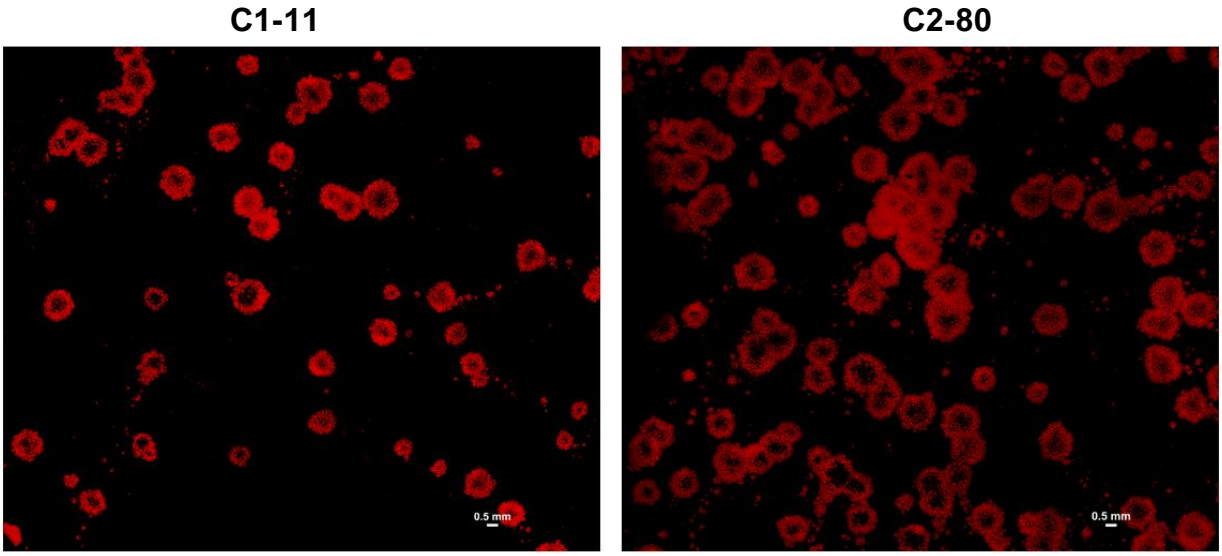

Figure 10: MRC5-grown C1-11 (left) and C2-80 (right) on rabbit skin cells results in uniform plaques.

Rabbit skin cells were infected with HSV-2 strains and incubated for 72 hours under human serum and MEM prior to indirect immunofluorescent staining. Anti-HSV antibody and a Cy5 fluor (shown in red) was used to image locations of HSV to observe the ring of infection around a focus. Both C1-11 and C2-80 strains show large, round plaques that are relatively uniform throughout. This allows for relatively easy quantification of titer as small, dense plaques are less likely to be missed during counting. The scalebar indicates 0.5 mm, and this is a 7x7 stitched image of the whole 35 mm plate.

The apparent titer of MRC5-based strains was about an order of magnitude higher in rabbit skin cells than in Vero cells (table 2). This means that the amount of viruses loaded onto the Western blot for the MRC5-grown stocks were ten times higher than for the Vero-grown stocks, explaining why the MRC5-Vero samples seemed to have a higher amount of viral proteins, even though they had smaller plaques.

Table 2: MRC5-grown strains have greater titer in rabbit skin cells (RSC).

	Titer in Vero cells	Titer in Rabbit skin cells	RSC titer : Vero titer
C1-11 Vero	1.6×10^8 PFU/mL	1.3×10^7 PFU/mL	0.081
C1-11 MRC5	8.3×10^5 PFU/mL	1.4×10^7 PFU/mL	17
C2-80 Vero	4.4×10^8 PFU/mL	1.0×10^8 PFU/mL	0.22
C2-80 MRC5	5.0×10^6 PFU/mL	7.0×10^7 PFU/mL	14

Vero cells and rabbit skin cells were infected with each MRC5-grown and Vero-grown strains and incubated for 72 hours under methyl cellulose and DMEM (for Vero cells) or MEM (for rabbit skin cells). The cells were then stained with methylene blue in methanol and observed to count PFUs. The titer of MRC-5 grown C1-11 and C2-80 increases by about one order of magnitude in rabbit skin cells as shown in the last column, indicating that the titer may have been inaccurately determined in Vero cells.

In both Vero and rabbit skin cells, strain C2-80 consistently had a higher titer than strain C1-11, relating to its ability to flourish in different host environments (table 2). To compare the ability to create successful infection in a new host, the MRC5-grown C1-11 and C2-80 strains were passaged through rabbit skin cells, and then titered on Vero cells to quantify PFU concentration (figure 11). Essentially, at each passage, the strains were introduced to a new host cell type. At the end of the experiment, the strain C2-80 consistently had a higher titer than C1-11, confirming initial observations.

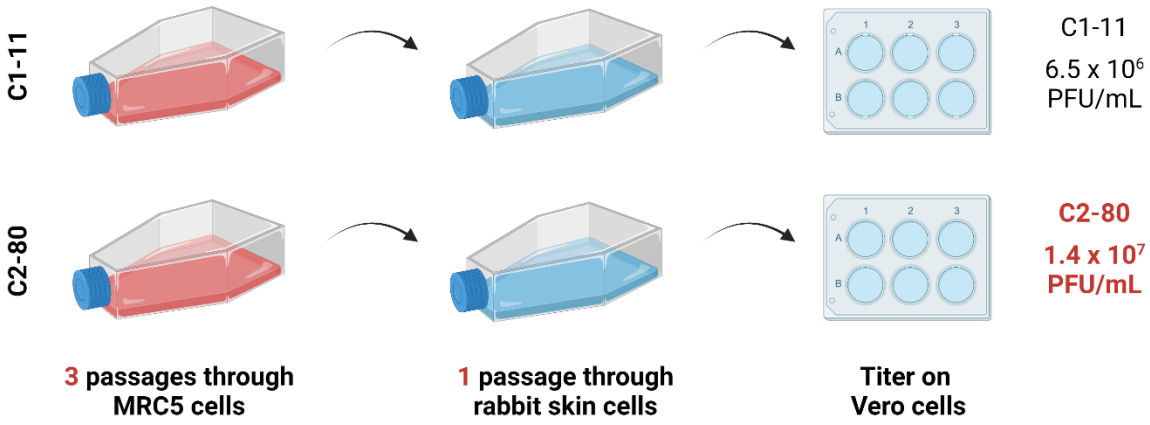

Figure 11: C2-80 shows superior adaptability to new host environments.

A test of adaptation was performed by using MRC5-grown strains of C1-11 and C2-80, which were relatively well adapted to their MRC5 host cell after 3 consecutive passages in the mini, master, and working stocks. The strains were then passaged through rabbit skin cells for a 72 hour infection at the same MOI, and then titered on Vero cells. At each stage, the strains were introduced to a new host environment to understand how effective they were in replicating in the new host. Strain C2-80 had a higher titer at the end of the experiment at 1.4 x 10^7 PFU/mL, compared to C1-11 with a titer of 6.5 x 10^6 PFU/mL. Image created using BioRender.

Visualization of C1-11 and C2-80 strains in Different Cells

Previously, the strains C1-11 and C2-80, whether grown on MRC5 or Vero cells, were grown on Vero cells to observe virus behavior. Viruses tend to behave differently based on the cell type they are grown in. For instance, one strain C1-11 (grown in MRC5 cells) looks vastly different in three unique cell types: Vero cells, rabbit skin cells, and MRC5 cells (figure 12).

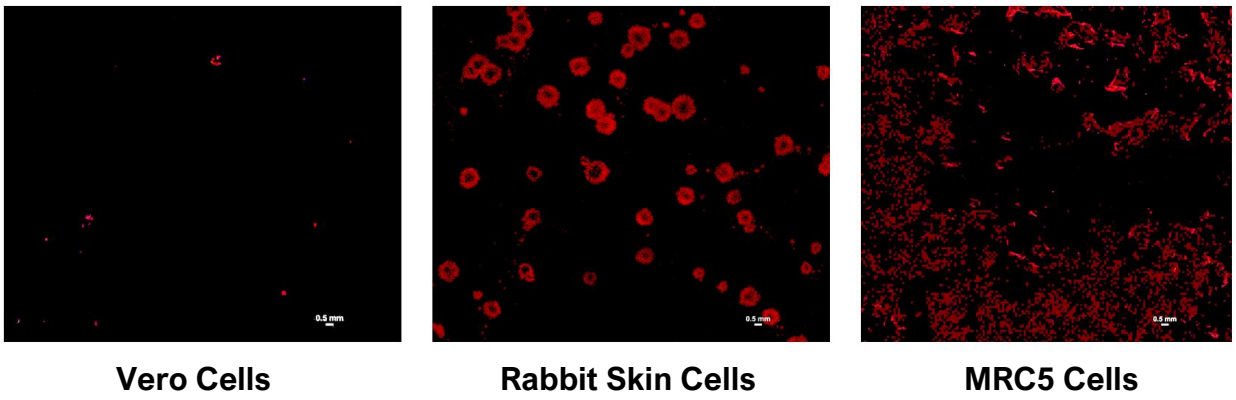

Figure 12: HSV-2 has distinct phenotypes dependent on cell type.

MRC5-grown C1-11 was grown on Vero, rabbit skin, and MRC5 cells to understand how phenotype changes between cell types for a single strain. All infections were incubated with the same number of PFUs for 72 hours prior to indirect immunofluorescent staining by anti-HSV antibody and Cy5 fluor. Cell to cell spread appears to increase from Vero cells to rabbit skin cells to MRC5 cells, indicating increased susceptibility to infection. The scale bar indicates 0.5 mm and each is a stitched 7x7 image of the whole 35 mm well.

Given that differences are seen between cell types, the same comparative experiments were carried out in a second cell type, MRC5 cells, to confirm initial observations. Though plaque assay and immunofluorescence imaging was performed on MRC5 cells, quantification of area was not accomplished due to the irregular borders of the plaques on MRC5 cells. Figure 13 shows Vero-grown and MRC5-grown strain C1-11 on MRC5 cells. Similar to the effect observed on Vero cells, the plaque size and spread area are larger when the strain is placed in a consistent host cell type. Strain C2-80 was not pictured as the MRC5 cells were very susceptible to this strain and sheared off the plate upon infection.

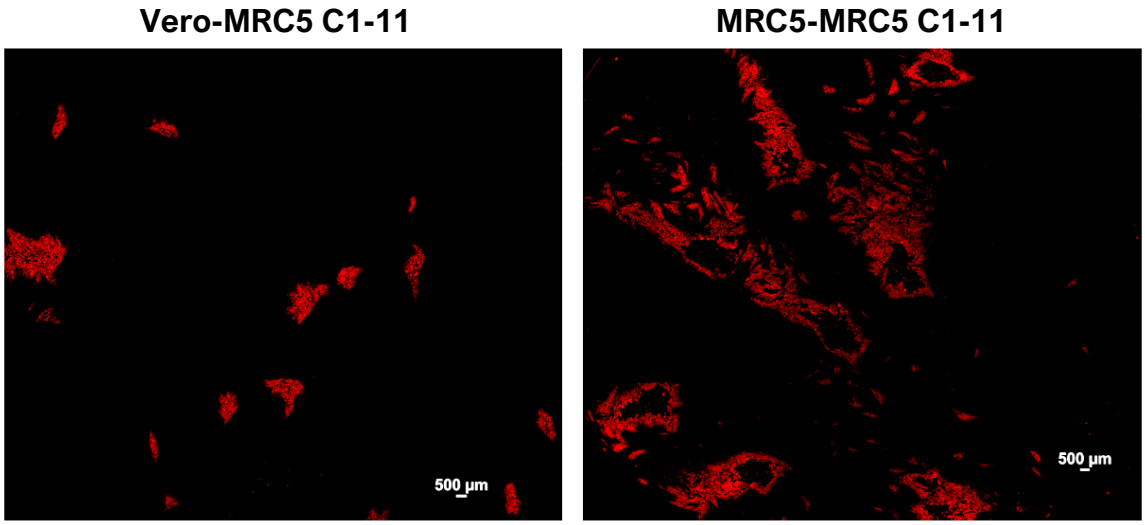

Figure 13: Comparison of Vero-grown C1-11 (left) and MRC5-grown C1-11 (right) shows adaptation in MRC5 cells leads to larger plaques and spread areas.

MRC5 cells were infected with HSV-2 strains and incubated for 48 hours under human serum and MEM prior to indirect immunofluorescent staining. Anti-HSV antibody and Cy5 fluor (shown in red) were used to image cell-cell spread of HSV. The Vero-grown C1-11 that is newly introduced into MRC5 cells shows smaller plaques with low cell-cell spread. The MRC5-grown C1-11 that is kept in a familiar host environment shows large plaques with extensive cell-cell spread. The scalebar indicates 500 µm and the images are of the whole 35 mm^2 plate, with 8x8 tiling and 4x zoom.

Comparison of the genomes of C1-11 and C2-80

Genomic analyses were conducted to understand intrastrain differences (mutations that arise from environment) and interstrain differences (between C1-11 and C2-80). For strain C1-11, the MRC5-grown and Vero-grown samples were compared to understand if there were any single nucleotide differences (SNPs) that arose as a result of the different culturing conditions. There were no detected SNPs in the consensus genomes between the MRC5-grown and Vero-grown samples. Thus, the differences seen in the phenotype between the MRC5-grown and Vero-grown strains may be due to non-genetic factors. For strain C2-80, the MRC5-grown and

Vero-grown samples were compared against the directly received sample that had not been cultured at all. In this comparison, there was one SNP found in the UL47 exon. In the direct received sample and MRC5-grown sample, the consensus nucleotide was T, but this had mutated to G in the consensus genome of the Vero-grown sample. UL47 is a tegument protein in the viral capsid, and has been shown to be essential for nuclear egress[13].

When MRC5-grown samples of C1-11 and C2-80 were compared, 118 SNPs were found, 93 of which were in the coding regions of the genes. The gene with the largest difference was in the UL36 gene with 10 SNPs, which also happens to be the largest gene in the HSV-2 genome. UL28, UL39, and UL49 also were largely different with 6-7 SNPs in each of the genes. When C1-11 and C2-80 were placed on a genome network graph, they mapped relatively close to each other. This means that in comparison to a larger pool of neonatal HSV-2 strains, strains C1-11 and C2-80 have relatively little differences in sequence.

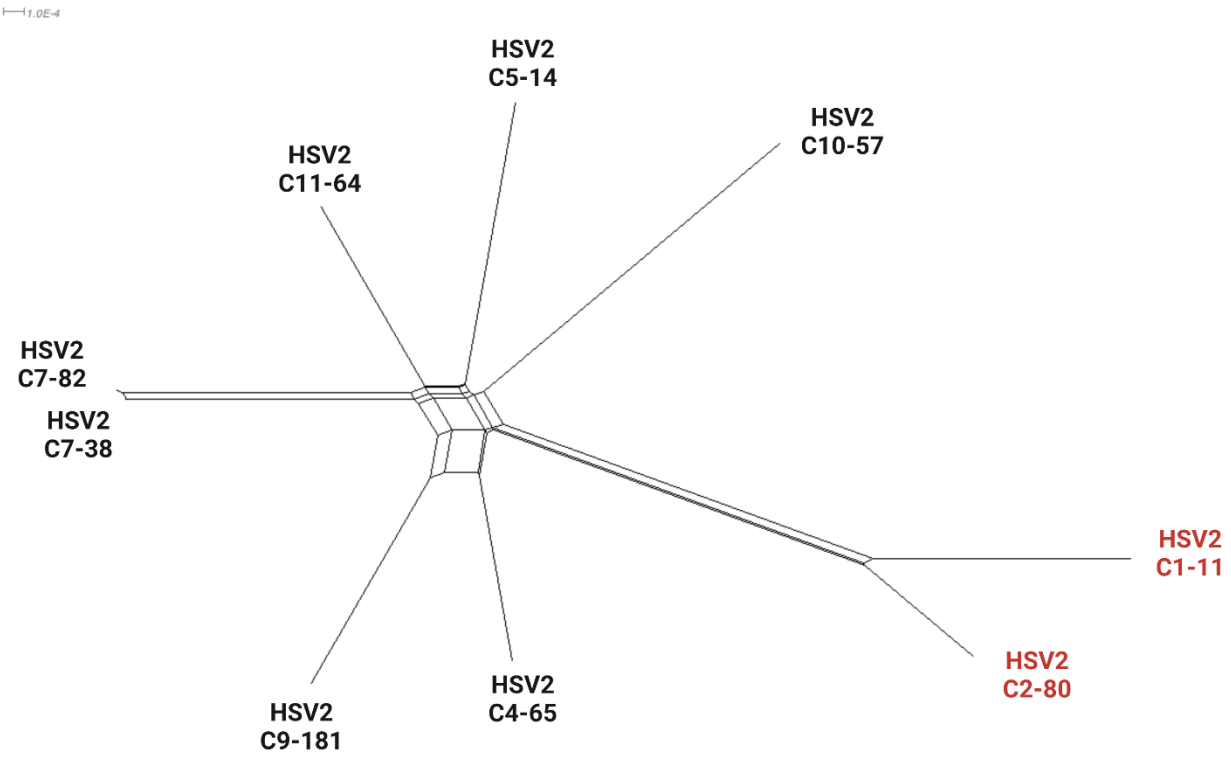

Figure 14: Gene network map reveals close genetic proximity of C1-11 and C2-80 strains.

The whole genome sequence of MRC5-grown C1-11 and C2-80 (in red) were aligned against seven other neonatal HSV-2 strains using the SplitsTree software. The scale bar indicates a distance that signifies the number of mutations per nucleotide position (1.0×10^{-4}). Strains that are closer together in distance means they are more genetically similar. The webbing represents recombination events between ancestral strains to create the novel strains labelled. All strains that are compared in this network graph were grown on MRC5 cells prior to sequencing.

Chapter 3

Discussion and Conclusions

Effect of Host Environment on Viral Behavior

Previous studies have shown that viral evolution does take place *in vitro*, but it is unknown how quickly these viruses evolve under laboratory conditions[10]. This study found that within three passages, the plaque size and cell-cell spread significantly increases for both strains examined here, C1-11 and C2-80. When strain C1-11 was passaged in Vero cells consistently (Vero-Vero), they formed much larger plaques in Vero cells compared to the strain that was passaged through MRC5 cells and newly placed on Vero cells (MRC5-Vero). The same pattern was shown for the C2-80 strain, with a relatively large area for the Vero-Vero samples and a smaller area for the MRC5-Vero samples. In addition to the plaque sizes, the observed cell-cell spread area increased for the samples that had been consistently grown in Vero cells. This suggests that maintaining a consistent environment in the early passages of the clinical isolates influences phenotype in laboratory cell culture.

There were a few limitations to this method, such as the accuracy of comparing plaque size to cell-cell spread area. The two assays were performed in the same timeline with 72 hour infections, but they were carried out in different media. The plaque-area assay was conducted under methyl cellulose, a viscous medium that restrain viral particles to a localized area. The cell-cell spread assay was conducted under liquid media with 1% human serum, which uses the antibodies to limit viral spread through the media while still allowing local virus spread via adjacent cells. Since HSV is a common virus in the population, the pooled human serum should contain a significant number of anti-HSV antibodies to limit the spread of the virus beyond its

initial plaque. However, there were several smaller plaques surrounding a large plaque in the images (figure 7), which may indicate that this method was not completely successful at restraining virus spread through the media. The same methyl cellulose media could not be used due to high background signal in the indirect immunofluorescence assay. The indirect immunofluorescence assay may need further optimization to limit viral spread during the growth period.

The Western blot was attempted to learn whether these changes were a result of higher viral load or faster replication. Contrary to expectations, the MRC5-Vero samples seemed to have a higher viral load as shown by the darker bands in Figure 9. However, the titer for the MRC5-Vero samples was later shown to be inaccurate by re-assessing the number of plaques on rabbit skin cells. In comparison to Vero cells, the rabbit skin cells showed a titer that was more than ten-fold higher for the MRC5-grown strains. That means that the MRC5-Vero samples loaded on the Western blot likely had ten times more input of plaque forming units than the Vero-Vero samples. Due to the difference in calculated viral titers, it is difficult to understand whether adaptation leads to higher viral loads or simply leads to faster spread.

The genomic analysis revealed that only C2-80 had a SNP in the Vero-grown sample in comparison to the direct received (uncultured) and MRC5-grown sample. Since this SNP was detected after passaging on Vero cells, it is likely due to the adaptation of the viruses to the Vero cells. The effect of the SNP was not determined, as further analysis of the coding region must be performed to understand what amino acid changes occur as a result. Since there were no detected SNPs in the consensus genome of C1-11 between the MRC5-grown and Vero-grown samples, the phenotypic changes seen through adaptation may not be due to genetic changes in the consensus genome. Comparing the consensus genome may not paint a complete picture of viral

evolution. This means that only the most common alleles present in the majority of a viral population were compared. It does not show minor variants, or the nucleotides that represent a minority of the viral population. In humans, minor variants play a large role in the viral diversity in a host, leading to host adaptation and changes in transmission behavior[14]. Further analysis of minor variants may reveal changes in how minor variants become a dominant nucleotide through selection in a laboratory setting. Studying which minor variants were selected for may reveal patterns of viral evolution for each strain.

In addition to viral factors, it is possible that parts of the host cell that are enabling this evolution in phenotype. As shown in figure 12, it was observed that one strain (MRC5-grown C1-11) can have three drastically different phenotypes in three different host cell types. Vero cells, lacking an interferon response, provided a baseline observation of viral behavior without immune interference, but showed the least amount of viral spread. Rabbit skin cells and MRC5 cells, especially, showed greater permissivity as the virus was able to spread further and cause greater cell death. This may be because of interferons in cell culture as these anti-viral compounds alert nearby cells to undergo apoptosis when infected. Fibroblasts are especially sensitive to interferons due to its anti-growth effect[15]. Another host factor that contributes to viral infection may be the profile of receptors expressed at the plasma membrane of the host cell. Expression of certain phosphatidyl serine receptors have been shown to influence viral tropism in different host cells due to differences in the efficiency of uptake[16]. Research has not been performed to show this phenomenon for herpes simplex viruses, but because they are enveloped viruses, it is likely that these host receptors would impact the efficiency of entry by receptor attachment[16]. Herpesviruses have a wide range of permissive hosts because of their multiple glycoproteins for entry, alternative entry pathways, and multiple alternative host receptors[17]. Due

to the versatility of herpesviruses, it is plausible that there may be currently unknown host factors that contribute to viral adaptation, rather than viral factors.

Observations of early adaptation of HSV-2 strains to different cell types in culture reveals the importance of maintaining consistent environmental conditions, especially when transitioning a clinical isolate into the laboratory. Currently, laboratories studying herpes simplex viruses have different protocols of growing viruses in the lab[18]. They may use different cells and reagents, which are likely to introduce differences in observed virus behavior between labs. Having different growth conditions for the same strain and comparing them would yield unreliable results as the strains are likely to adapt to a particular host differently. This does present a challenge in our field, as clinical isolates must be kept at a low passage to minimize the appearance of lab adaptation impacts.

Comparison of C1-11 and C2-80 as Disseminated Strains

Strains C1-11 and C2-80 have similar clinical profiles, as they resulted in a disseminated infection in neonates within two weeks of birth. When the strains were placed into Vero cells after initial propagation in MRC5 cells, they both grew very small plaques. However, when the Vero-Vero samples were compared, there was a significant difference between the two groups where the C2-80 grew larger than the C1-11 strain. In addition to its larger size, it consistently had a higher titer (table 2). Even when the strain was grown through three different cell types, C2-80 had a titer that was two times higher than C1-11 (figure 11). These strains were grown for the same amount of time with the same amount of starting PFUs, indicating that C2-80 may be more successful by creating more infectious particles in a susceptible host. Interestingly, strain

C1-11 had a larger ratio of spread area to plaque area when it had been consistently passaged in Vero cells (Table 1). This means that as it adapts to a new environment over several passages, the area of spread increases disproportionately greater than its plaque size.

When the consensus genomes of the two strains were compared, many SNPs were found in UL28, UL36, UL39, and UL49. UL36 and UL49 are two genes that encode proteins in the tegument layer. In HSV-1, UL49 was shown to play a role in viral spread in mouse models and UL36 was shown to play a role in dampening the interferon responses in hosts[19,20]. UL28 plays a role in virion assembly as it is part of the terminase complex that packages the genome inside the capsid[21]. UL39 is part of the ribonucleotide reductase complex, and mutations in this gene have shown to impair the pathogenesis of HSV-1[22]. The culmination of these genetic differences may be the result of the different viral fitness *in vitro*. It is possible that these genomic differences contribute to the ability of the viral particles to replicate faster in a host, but further studies are needed to confirm that these genomic changes are causing such differences.

Many differences between C1-11 and C2-80 exist, such as viral load, plaque phenotype, and genome, but it does not explain why they have a similar clinical outcome. This suggests that there are many other factors at play, such as host factors and the conditions of the initial infection. Many host pathways have been shown to be dysregulated by HSV-1 infection in neuronal cells[23]. The interaction between a particular strain of HSV and a particular host is very specific and would dictate the outcome of infection[23]. If different hosts have mutations that lead to differences in signaling pathways, it may alter the outcome of the infection. There are also factors relating to the circumstance of infection affecting neonatal HSV risk factors. During birth, the disruption of rupture of membranes or the disruption of the cutaneous barrier are risk

factors that may increase the chances of neonatal HSV disease.[24] The time of exposure may also play a role, as exposure *in utero* can lead to microcephaly[24].

Clinical severity of infection occurs in a spectrum ranging from mild skin lesions to brain inflammation. This adaptation study showed that strains that come from infections of similar severity can have differences in their adaptive ability, enabling us to tease out nuanced differences between strains. These differences may be critical to understanding the factors that contribute to virulence of HSV-2 infections. For this preliminary study of adaptation, only two strains were compared to understand if there would be any differences in viral adaptation. Since the study has shown significant differences in viral behavior through different host cell types, the sample of clinical isolates will be expanded to include strains coming from CNS and SEM infections. Developing a robust phenotypic profile of these neonatal strains with a large sample size is more likely to be accurate in detecting associations between cell culture phenotypes and the severity of symptoms in newly infected neonates.

Chapter 4

Materials and Methods

Mammalian Cell Culture

Three different mammalian cell types were used in the series of experiments: African green monkey kidney cells (Vero cells), human lung fibroblast cells (MRC5 cells), and rabbit skin cells. These cells were maintained as a monolayer in T-150 culturing flasks in a 37C incubator. Vero cells were incubated in Dulbecco's Modified Eagle Medium (ThermoFisher) with 10% fetal bovine serum (ThermoFisher), 1X L-glutamine (ThermoFisher), and 1X penicillin/streptomycin (ThermoFisher). MRC5 cells were grown in Minimum Essential Medium (Sigma) with 10% fetal bovine serum, 1X L-glutamine, 1X penicillin/streptomycin, and G5 fibroblast growth factor (Thermofisher). Rabbit skin cells (an established cell line) were incubated in Minimum Essential Medium with 5% newborn calf serum (Sigma), 1% L-glutamine, and 1% penicillin/streptomycin. When all cells reach 90% confluency, they were passaged into a new T-150 flask. The original media in the flasks was aspirated to remove waste products, and the cells were washed with phosphate buffered saline (PBS). After PBS was aspirated, trypsin was applied to the monolayer and incubated in 37C for 5-10 minutes to release the adherent cells from the flask. Trypsin was then neutralized by diluting it five-fold with media. The loose cells were then collected in a 50 mL conical and centrifuged for 2 minutes at 1000 rpm to pellet the cells. The remaining media/trypsin mixture was aspirated and the remaining cell pellet was resuspended in fresh media (15 mL for Vero cells, 10 mL for rabbit skin cells, and 5 mL for MRC5 cells). New flasks were seeded with 1 mL of the cell suspension and 24 mL of fresh media, then incubated in 37C until it reached 90% confluency.

For titering and imaging infections, Vero cells, MRC5 cells, and rabbit skin cells were seeded onto 6-well dishes each with a 35 mm diameter to achieve full confluency over a 24 hour period. The remaining resuspended cells from cell passaging were counted with a hemocytometer to seed a density of 4×10^5 cells per well for Vero cells, 1×10^6 cells per well for rabbit skin cells, and 6×10^5 cells per well for MRC5 cells. A solution made with 1-part resuspended cells, 1-part trypan blue, and 3-parts media was loaded onto the hemocytometer to count the number of live cells under a light microscope. The following formula was used to calculate cell density:

(Number of live cells / 4) x dilution factor (5) x 10,000 = n cells/mL

The required number of cells was calculated based on the number of wells needed for each experiment. Using the calculated cell density and the number of cells required, the volume of cells was calculated and transferred to a new flask. The volume was brought up with fresh media to have 2 mL of cell suspension for each well. The seeded 6-plate wells were incubated for 24 hours at 37C for a confluent monolayer.

In-vitro Growth of HSV-2

Clinical HSV-2 strains were grown from leftover diagnostic samples of neonatal HSV infections received from our collaborator, Dr. Lisa Akhtar at Northwestern University Feinberg School of Medicine. The samples were collected from serum or plasma. 10 uL of each HSV-2 sample was put into a confluent monolayer of Vero cells and MRC5 cells in a 35 mm dish for 1 hour in a 37^{o}C incubator. The sample was then aspirated from the cells, and replaced with a layer of media with 2% FBS to allow the viral growth for 72 hours. A lower concentration of FBS was

used during the viral growth period to slow down cell growth. The cell and virus solution was collected, sonicated for 10 seconds, and titered on Vero cells. The mini-stock solution was seeded onto a flask of Vero or MRC5 cells at a multiplicity-of-infection (MOI) of 0.01, consistent with the cell type they were placed into for the mini-stock. The infection was carried out in the same manner with a 1-hour long infection and 72 hour growth period to create the master stock. The master stock was then sonicated for 10 seconds and titered on Vero cells. This process was repeated once more to create the working stock of each strain at a MOI of 0.01. The initial propagation was carried out by Chris Bowen prior to the start of this project.

Titering was performed using a confluent monolayer of Vero cells on six-well plates of 35 mm. Each virus sample was prepared by 6 serial ten-fold dilutions in DMEM with 2% FBS, 1X penicillin/streptomycin, and 1X L-glutamine. The solutions that were diluted 10^4, 10^5, and 10^6-fold were placed on each well in duplicate to cover the surface of the cells. The Vero cells were incubated with the infectious particles for 1 hour at 37ºC. The virus solution was then aspirated and replaced with methylcellulose and DMEM to grow for 72 hours at 37ºC. The methylcellulose solution is a viscous liquid that restrains viral movement in liquid so that it cannot freely spread to neighboring cells. After this 72-hour growth period, the methylcellulose media was aspirated. The cells were rinsed with PBS and stained with 1% methylene blue in methanol overnight. After the staining, the number of viral plaques were counted under a dissection microscope (Olympus) to calculate the number of plaque forming units (PFU) in a given working stock.

Titering on rabbit skin cells and MRC5 cells were performed in the same manner but using methylcellulose and MEM. MRC5 cells were grown during 48 hour incubation period (instead of 72 hours) and were stained with crystal violet (Electron Microscopy Sciences).

Immunofluorescent Assay

Similar to the titering process, viral dilutions were prepared by serial ten-fold dilutions and were placed on a confluent layer of cells in a 6-well plate for one hour. Once the hour-long infection was over, the viruses were aspirated and replaced with media corresponding to each cell type with 1% human serum. The monolayer of cells were then incubated for 72 hours for Vero cells and rabbit skin cells, or 48 hours for MRC5 cells. After this infection period, the media was aspirated from cells and washed with PBS. The cells were fixed with 4% paraformaldehyde and permeabilized with 0.5% Triton-X (Fisher BioReagents). After washing, a 3% normal goat serum solution in PBS was used to reduce background signals prior to antibody staining. The rabbit anti-HSV antibody (Dako) was made up at a 1:500 dilution and incubated with the cells overnight at 4^{o}C in a humid chamber. The first antibody was removed and the cells were washed with PBS. A goat-anti-rabbit antibody with a Cy5 fluorescent tag (Invitrogen) was used at a 1:250 dilution and incubated with the cells at room temperature for one hour in a dark area. The antibodies were washed off and imaged in a dark room.

Images of the plaques in the titering assays and the immunofluorescent assays were taken with the Nikon microscope. To image the whole well, a large image was stitched using the NIS Elements software with a 8 by 8 dimensions at a 4x optical zoom.

Image Analysis

The ImageJ software was used to analyze the images using the region of interest tool. The border of a plaque or fluorescent area was traced to calculate the area in mm^2. The pixel size was calibrated to the true distance provided by the NIS Elements Software to calculate the area of a

plaque from the titering assay and the area of viral spread from the immunofluorescent assay. For each sample, the mean area of the plaque and spread were calculated, along with its standard deviation.

Western Blot

To collect samples for Western blot, each viral working stock was used to create an infection at an MOI of 0.01 in DMEM with 2% FBS. The infection was performed on a confluent monolayer of Vero cells in a 6 well plate for 24 hours. If after this period, the cells were floating, the media was collected in mini-centrifuge tubes and spun down. If the cells were still adherent, the media was aspirated. The cells were then washed with ice-cold PBS. RIPA buffer (Thermofisher) with a protease tablet (Thermofisher) and DTT (Thermofisher) were placed onto the wells prior to scraping the cells off. The scraped solution was placed into mini-centrifuge tubes, sonicated for 4 seconds, and shaken for 15 minutes at 4^{o}C. They were then spun at 15000xg in a centrifuge for 10 minutes at 4^{o}C. The pellet at the bottom of the tube containing cell debris was removed by pipetting out the pellet. The supernatant was transferred to clean tubes prior to use. The protein content of each supernatant sample was analyzed by BCA assay to normalize the amount of total protein analyzed on an SDS-polyacrylamide gel.

The gels were casted at a 10% solution of polyacrylamide (Bio-Rad) with N,N,N’N’-tetramethyl-ethylenediamine (Sigma) and APS (BioRad), and were incubated overnight in a humid chamber at 4^{o}C to solidify. To prepare the samples to run, 20 ng of protein was aliquoted and incubated with Laemmli buffer in a 3 to 1 ratio at 95^{o}C for 5 minutes. The samples were loaded onto the wells and run for 10 minutes at 50V and 60 minutes at 100V. The gel was placed

onto a nitrocellulose paper, sandwiched between layers of foam during the wet transfer for 16 hours at 30V. The nitrocellulose membrane was then placed into a dark chamber to block with 5% milk (Lab Scientific) for an hour at room temperature. The rabbit anti-HSV antibody (Dako) was placed into a solution with 1% milk and placed onto the membrane overnight at 4^{o}C. The primary antibody was removed and the membrane was washed with TBS-T prior to adding the goat-anti-rabbit secondary antibody conjugated with peroxide (Pierce) in 1% milk solution. The membrane was developed using horseradish peroxidase enzyme (Pierce ECL Western Blotting Substrate) and was visualized shortly after on a ChemiDoc XRS+ (Bio-Rad). A control blot was performed simultaneously to blot for GAPDH using the rabbit anti-GAPDH primary antibody.

Genome Analysis

The viral genomes were prepared by Chris Bowen and compiled by Daniel Renner and Sarah Dweikat prior to the start of the project. Viral samples from the master stock were processed by DNA extraction and quantification, followed by shearing into 500-1000 base pair fragments for library preparation. HSV-2 DNA was enriched and amplified prior to sequencing with an Illumina MiSeq.

Genomic analysis was initially carried out in the AliView software to understand if there were any differences that arose as a result of culturing method. For strain C2-80, the direct-received (uncultured sample), MRC5-grown sample, and Vero-grown sample were aligned to detect single nucleotide differences or insertions and deletions. For strain C1-11, the MRC5-grown strain and the Vero-grown strains were compared against each other due to lack of enough

sample to sequence without culturing. When differences were found, the sequences were then aligned in the Geneious software to understand where in the genome the mutations were found.

When looking for differences in the sequence of C1-11 and C2-80 in Geneious, the MRC5-grown strains were compared against each other for consistency. In addition, the MRC5-grown C1-11 and C2-80 were mapped in a genome network graph with other HSV-2 strains to understand their genomic proximity to each other. The SplitsTree software was used to align multiple sequences of HSV-2. The network is then mapped to show genetically similar strains closer to each other on this network.

Statistics

Comparisons of significance between MRC5-Vero groups and between strains C1-11 and C2-80 were performed in Excel via a two-sampled T-test assuming unequal variance.

BIBLIOGRAPHY

1. Fleming, D. Herpes Virus Type 2 Infection and Genital Symptoms in Primary Care Patients. *Sex. Transm. Dis.* **33**, 416–421 (2006).

2. Whitley, R. J. *et al.* Changing presentation of herpes simplex virus infection in neonates. *J. Infect. Dis.* **158**, 109–116 (1988).

3. Looker, K. J. *et al.* First estimates of the global and regional incidence of neonatal herpes infection. *Lancet Glob. Health* **5**, e300–e309 (2017).

4. James, S. H. & Kimberlin, D. W. Neonatal Herpes Simplex Virus Infection: Epidemiology and Treatment. *Clin. Perinatol.* **42**, 47–59 (2015).

5. Cernik, C. The Treatment of Herpes Simplex InfectionsAn Evidence-Based Review. *Arch. Intern. Med.* **168**, 1137 (2008).

6. Szpara, M. L. *et al.* Evolution and Diversity in Human Herpes Simplex Virus Genomes. *J. Virol.* **88**, 1209–1227 (2014).

7. Kuny, C. V. & Szpara, M. L. Alphaherpesvirus Genomics: Past, Present and Future. in *Alphaherpesviruses: Molecular Biology, Host Interactions and Control* 41–80 (Caister Academic Press, 2020). doi:10.21775/9781913652555.01.

8. Muggeridge, M. I. Characterization of cell-cell fusion mediated by herpes simplex virus 2 glycoproteins gB, gD, gH and gL in transfected cells. *J. Gen. Virol.* **81**, 2017–2027 (2000).

9. Mao, H. & Rosenthal, K. S. Strain-Dependent Structural Variants of Herpes Simplex Virus Type 1 ICP34.5 Determine Viral Plaque Size, Efficiency of Glycoprotein

Processing, and Viral Release and Neuroinvasive Disease Potential. *J. Virol.* **77**, 3409–3417 (2003).

10. Kuny, C. V., Bowen, C. D., Renner, D. W., Johnston, C. M. & Szpara, M. L. In vitro evolution of herpes simplex virus 1 (HSV-1) reveals selection for syncytia and other minor variants in cell culture. *Virus Evol.* **6**, (2020).

11. Ammerman, N. C., Beier-Sexton, M. & Azad, A. F. Growth and Maintenance of Vero Cell Lines. in *Current Protocols in Microbiology* (eds. Coico, R., Kowalik, T., Quarles, J., Stevenson, B. & Taylor, R.) (John Wiley & Sons, Inc., 2008). doi:10.1002/9780471729259.mca04es11.

12. Akhtar, L. N. *et al.* Genotypic and Phenotypic Diversity of Herpes Simplex Virus 2 within the Infected Neonatal Population. *mSphere* **4**, e00590-18 (2019).

13. Liu, Z. *et al.* Herpes Simplex Virus 1 UL47 Interacts with Viral Nuclear Egress Factors UL31, UL34, and Us3 and Regulates Viral Nuclear Egress. *J. Virol.* **88**, 4657–4667 (2014).

14. Rathbun, M. M. *et al.* Comparison of herpes simplex virus 1 genetic diversity between adult sexual transmission partners with genital infection. *PLOS Pathog.* **18**, e1010437 (2022).

15. Richtsmeier, W. J., Johns, M. E., Cantrell, R. W. & Sorge, K. Interferon sensitivity of fibroblast cell cultures derived from patients with neoplasms of the head and neck. *Otolaryngol.--Head Neck Surg. Off. J. Am. Acad. Otolaryngol.-Head Neck Surg.* **93**, 492–499 (1985).

16. Moller-Tank, S. & Maury, W. Phosphatidylserine receptors: Enhancers of enveloped virus entry and infection. *Virology* **468–470**, 565–580 (2014).

17. Karasneh, G. A. & Shukla, D. Herpes simplex virus infects most cell types in vitro: clues to its success. *Virol. J.* **8**, 1–11 (2011).

18. Grosche, L. *et al.* Herpes Simplex Virus Type 1 Propagation, Titration and Single-step Growth Curves. *Bio-Protoc.* **9**, e3441 (2019).

19. Wang, S., Wang, K., Li, J. & Zheng, C. Herpes Simplex Virus 1 Ubiquitin-Specific Protease UL36 Inhibits Beta Interferon Production by Deubiquitinating TRAF3. *J. Virol.* **87**, 11851–11860 (2013).

20. Duffy, C. *et al.* Characterization of a UL49-Null Mutant: VP22 of Herpes Simplex Virus Type 1 Facilitates Viral Spread in Cultured Cells and the Mouse Cornea. *J. Virol.* **80**, 8664–8675 (2006).

21. Heming, J. D., Huffman, J. B., Jones, L. M. & Homa, F. L. Isolation and Characterization of the Herpes Simplex Virus 1 Terminase Complex. *J. Virol.* **88**, 225–236 (2014).

22. Mostafa, H. H. *et al.* Herpes Simplex Virus 1 Mutant with Point Mutations in UL39 Is Impaired for Acute Viral Replication in Mice, Establishment of Latency, and Explant-Induced Reactivation. *J. Virol.* **92**, e01654-17 (2018).

23. Mangold, C. A., Rathbun, M. M., Renner, D. W., Kuny, C. V. & Szpara, M. L. Viral infection of human neurons triggers strain-specific differences in host neuronal and viral transcriptomes. *PLOS Pathog.* **17**, e1009441 (2021).

24. Pinninti, S. G. & Kimberlin, D. W. Neonatal herpes simplex virus infections. *Semin. Perinatol.* **42**, 168–175 (2018).

ACADEMIC VITA

Ellie Kim

EDUCATION

Pennsylvania State University, Schreyer Honors College University Park, PA 16802
Bachelor of Science in Biochemistry and Molecular Biology May 2023
Bachelor of Musical Arts with Piano Application

PAPERS & PRESENTATIONS

Kim, E., Kim, M. "Development of a Culturally and Linguistically Appropriate Chatbot to Promote HPV Vaccination Among Korean Americans." **US-Korea Conference**, August 17-20, 2022. Poster Presentation

Kim, Forney, Viel, Keddari, O'Brien, Nelson, Gecaine, Zabeti, Weirauch, Kottyan. "Enrichment of Epstein-Barr Virus in Patients with Multiple Sclerosis." **American Association for Immunology**, May 6-10, 2022. Poster Presentation.

Max Urbanczyk, Athar Abuhelou, Julia Marzi, **Ellie Kim**, Shannon Layland, & Katja Schenke-Layland. "Investigating the influence of organ-specific endothelial cells for diabetes research in a bioreactor setup." Manuscript in preparation.

Kim, Dweikat, Rathbun, Szpara. "Investigating structural components of glycoprotein B to assess virulence of herpes simplex virus 1." **International Conference for Undergraduate Research**, September 28, 2021. Oral Presentation.

Kim, Forney, Viel, Keddari, O'Brien, Nelson, Gecaine, Zabeti, Weirauch, Kottyan. "Enrichment of Epstein-Barr Virus in Patients with Multiple Sclerosis." **Cincinnati Children's Hospital Medical Center SURF Symposium**, July 28, 2021. Oral Presentation; Honorable Mention.

Ellie Kim*, Elizabeth Handorf*, Jamaiica Hurston*, Yasine Keddari*, Sherry Thornton, Lori Crosby, Leah Kottyan, Cindy Bachurski, Jessica Kahn, and Jamilah Hackworth. Best practices for mentoring undergraduate researchers in academic health centers. Manuscript Submitted. *co-first authors.

Kenyatta Viel, Marissa Granitto, Carmy Forney, **Ellie Kim**, Yasine Keddari, Madison O'Brien, Catrina Nelson, Paul Gecaine, Aram Zabeti, Matthew Weirauch, Leah Kottyan. Role of Epstein-Barr Virus type I and II in the genetic etiology of Multiple Sclerosis. Manuscript in Preparation.

Kim, Dweikat, Rathbun, Szpara. "The Effect of Glycoprotein B Mutants on the Fusion of Herpes Simplex Virus 1 to Mammalian Host Cells." **Allegheny Branch American Society for Microbiology**, November 14, 2020. Poster.

RESEARCH EXPERIENCE

Oliver (Immunology) Lab, University of Pennsylvania/Children's Hospital of Philadelphia Jun 2022 – Aug 2022

Conducted experiments to study the role of Cul5 E3 ubiquitin ligase in regulating hematopoietic cell differentiation and proliferation through the CHOP Research Institute Summer Scholars Program (CRISSP)

Learned essential technologies in immunology, such as flow cytometry, FACS, and colony formation assays

Schenke-Layland Lab, Eberhard Karls University of Tübingen Aug 2021 – Nov 2021

Coordinated experiments to establish a coculture system between endothelial cells and pancreatic cells to improve functionality of both cell types using a BioReactor system and quantitative PCR (qPCR) technologies

Received support from DAAD Research Internship in Science and Engineering and German Chemical Society

Kottyan/Weirauch Lab, Cincinnati Children's Hospital, Department of Immunology May 2021 – Jul 2021

Established preliminary association between Epstein-Barr Virus infection and the development of multiple sclerosis in patients using qPCR technologies

Received support from Cincinnati Children's Hospital Medical Center and Schmidlapp Young Women Scholars Fund

Virology (Szpara) Lab, Penn State University, Eberly College of Science
Jan 2020 - Present

Maintained mammalian cell cultures and conducted viral infections to study genotypic and phenotypic variations of neonatal herpesviruses for a thesis project

Elucidated the effect of structural variants of a herpesvirus-1 fusogen protein using PyMOL modeling software, in collaboration with experts in structural biology at Tufts university

Proposed methodology to observe the fusogenic impact of mutations in glycoprotein B on fusion with host cells

Neuroscience (Chen) Lab, Penn State University, Eberly College of Science Aug 2019 - Dec 2019

Assisted postdoctoral scholars in spinal cord neuro-regeneration to develop a therapy for amyotrophic lateral sclerosis (ALS) through spinal cord and brain slicing, tissue immunostaining, rodent dissection, and cell quantification

Biomechanics Lab, Penn State University, College of Health and Human Development Aug 2018 - May 2019

Participated in researching ACL reconstruction surgery techniques for injured children by creating 3D graphics of tibias and femurs using Avizo software, 3D printing the created graphics, and analyzing the accuracy of the models using Rhinoceros 3D software (computer-aided design)

Designed covers for inertial measurement units for pendulum-like wear by using Rhino 3D software and 3D printing designs of three different curvatures for a project in the Department of Industrial Engineering

Demonstrated the use of elastic energy in energy conservation during walking through a passive walking device by designing on Rhino 3D, assembling after printing, and analyzing its performance through motion capture and MatLab

WORK EXPERIENCE

Intensive English Communication Program Tutor
Jan 2022 – Present

Reviewed concepts in first year biology courses for exchange students in the KAUST Gifted Students Program

Morgan Academic Center Tutor
Oct 2020 – May 2021

Reviewed core concepts and reinforced study techniques for student athletes enrolled in organic chemistry and mechanics courses for two hours each week

Math, Science, and English Tutor for Middle and High School ESL Students
Feb 2020 – May 2021

Reinforced fundamental ideas in math and science subjects to improve understanding during the school year and introduced students to new concepts in geometry, precalculus, biology, and chemistry during the summer

Conducted weekly summer workshops consisting of debating, reading books, giving writing feedback to improve reading comprehension, essay writing, and persuasive skills for ESL students

HONORS AND AWARDS

Astronaut Scholarship
Mar 2022

One of 68 students to receive the national Astronaut Scholarship for excellence in research and leadership

Goldwater Scholarship
Jan 2022

One of two students at Penn State University to be awarded the National Goldwater Scholarship for excellence in research

DAAD RISE Fellowship
Aug 2021

Awarded funding to conduct research at the Eberhard Karls University of Tübingen (268 students/1635)

Cincinnati Children's Hospital Medical Center Summer Undergraduate Research Fellowship

May 2021

Awarded funding to conduct research at the Cincinnati Children's Hospital

Schmidlapp Young Women Scholars

May 2021

Awarded a scholarship to attend an immunology conference in May 2022 and to pursue academic interests (8 students/100+)

CHOP Research Institute Summer Scholars Program

Jun 2022

One of thirty students selected to perform research for the summer at the Children's Hospital of Philadelphia

UKC Technical Fellowship and FIRE Fellowship

Aug 2022

Fellowship awarded to trainees in STEM (undergraduate, graduate, and post-doctoral scholars) to present their research at the US-Korea Conference (UKC), as well as a second fellowship (Fostering Innovation in Rising Experts)

UKC 2022 Paper Award

Aug 2022

Awarded in recognition of an excellent abstract and presentation at the 2022 US-Korea Conference on Science, Technology, and Entrepreneurship

Brock Scholarship in Music

May 2022

Scholarship provided by the College of Arts and Architecture for students pursuing career-advancing opportunities during the summer

Evan Pugh Senior Award

May 2021

Awarded to students at Penn State University with excelling academic record

Student Engagement Network Grant

Sept 2020

Received financial support for undergraduate research in virology during the fall semester of 2020

President's Freshman Award

Apr 2020

Awarded to freshman students at Penn State University with excelling academic record

Eleanor Beane Award

Mar 2021

Awarded to a student demonstrating high skill in performance at the Penn State School of Music

Homer Braddock Scholarship

Aug 2019 – May 2023

4-year merit scholarship provided to students excelling in the STEM field, awarded by the Eberly College of Science

EXTRACURRICULAR ACTIVITIES

Vaccinate America, Penn State University
May 2020 – Present

Advocated the benefits of vaccination to improve the public health of the local community as President (2021-2022) and Vice President (2020-2021) through interactive presentations with parents in school districts across Pennsylvania

Spoke as a representative of Gen Z for a public education campaign "We Can Do This" led by US Dept. of HHS and the White House to promote vaccination among young adults and teens

Science LionPride, Penn State University
Feb 2020 – Present

Actively involved in outreach events for prospective students and alumni as ambassadors of the College of Science, such as student tours, alumni networking events, and fundraising for children with cancer

Mount Nittany Medical Center, Patient Floor Volunteer Oct 2017 – Mar 2020

Assisted medical staff by transporting patients, handling discharge, and transportation of materials

Took care of non-clinical needs of the patients to ensure a comfortable hospital stay

Trained incoming volunteers at least once a month to teach them the essential skills on each specific floor